Galaxy Alignment with Surrounding Large-Scale Structure

Undergraduate Research Thesis

Presented in partial fulfillment of the requirements for graduation with research distinction in Astronomy and Astrophysics in the undergraduate colleges of The Ohio State University

By
Dhvanil Desai

The Ohio State University
April 2020

Project Advisor: Professor Barbara Ryden, Department of Astronomy

Abstract

Using a sample of $\sim 400,000$ low redshift ($0.02 < z < 0.25$) spectroscopic galaxies from the Sloan Legacy Survey, I study the alignment of these targets with the distribution of their surrounding galaxies. With the average alignment angle of 45° being a random distribution, the luminous red galaxies show the highest parallel alignment (at a 9σ significance level) on average with their surrounding environment. When looking at the alignment of a luminous red target galaxy with its surrounding structure out to a projected distance r_p, the average alignment angle is constant at $\langle\phi\rangle \sim 44.3°$ in the interval 5 Mpc $< r_p <$ 30 Mpc. The faint red galaxies have a 4σ parallel alignment for $r_p \gtrsim 18$ Mpc but no significant alignment for smaller radii. Blue galaxies do not show significant alignment at any value of r_p. Alignment for any of the four subsamples shows no dependence on other properties such as the number of surrounding galaxies, or magnitude and direction of the mean position offset of the surrounding galaxies. Future studies of alignment as a function of redshift will help to constrain the interplay between galaxy evolution and the development of large-scale structure.

1 Introduction & Background

Study of the alignment of galaxies with each other and with large-scale structure has a long history[1]. Studying intrinsic alignments can shed light on how the large-scale structure affects the formation and evolution of galaxies. These interactions often depend on galaxy type. Some properties used to categorize galaxies are their color and luminosity. Red galaxies are usually elliptical, early-type galaxies. Relatively luminous blue galaxies are flat, disk-shaped, late-type galaxies with angular momentum (spin) support, and dimmer blue galaxies tend to be irregular in shape. Since the blue disks are rotationally supported, it is reasonable to assume some sort of alignment between the disks and the large-scale structure. As shown in several studies reviewed by Joachimi et al., blue disk galaxies tend to align their spin perpendicular to the direction of filaments in the large-scale structure[2]. However, this signal is fainter than the one seen in the red galaxies which tend to align their major axes with the direction of the filament[3]. There is a strong correlation between the mass and the luminosity of galaxies which shows that higher mass galaxies are higher in luminosity. Studies using simulations show that the more massive galaxies and massive dark-matter halos have stronger alignment signals[4]. This shows that massive objects tend

[1]Brown 1939; Wyatt and Brown 1955; Reaves 1958; Brown 1964; Joachimi et al. 2015.

[2]Joachimi et al. 2015.

[3]Chen et al. 2019; Joachimi et al. 2015.

[4]Ganeshaiah Veena et al. 2019.

to influence their surroundings more. Luminous red galaxies are massive and can align with their surroundings due to several processes. Being so massive, they can cannibalize the smaller galaxies in a preferred direction ending up aligning with their surroundings as they grow. Massive galaxies also influence their surroundings via tidal interactions. Tidal torquing can explain the preferred distribution of surrounding galaxies along the major axis of the massive central galaxy[5]. These are some of the ways alignments can be produced.

Besides the study of the large-scale structure, intrinsic alignments are extremely important for weak gravitational lensing measurements[6]. Weak gravitational lensing is a tool to probe the matter distribution in the universe using the bending of light due to gravity. It produces distortions in the shapes of galaxies being lensed. When the lensed galaxies have some kind of intrinsic alignment, it acts as a contamination in the actual weak-lensing signal. So, in order to properly isolate the real weak-lensing signal, it is important to understand how galaxies align and how the alignments depend on the properties of galaxies. The weak-lensing signal is stronger for high redshift galaxies due to the presence of more matter in the line-of-sight. General alignments with negligible weak-lensing effects for different types of galaxies can be understood by studying alignments for low redshift galaxies.

In Section 2, I will describe the selection of data from the Sloan Digital Sky Survey, the cuts on several parameters, noteworthy properties, explain target galaxies and surrounding galaxies, and finally split the sample of my target galaxies into four subsamples based on a luminosity dependent color divider. In Section 3, I will illustrate the process of defining the alignment angle necessary for this study using mathematical tools. Section 4 will show the results of my primary alignment analyses on four subsamples of target galaxies using statistical means, and the dependence of alignment on luminosity for red and blue galaxies. Section 5 will go into the detail of how the average alignment angle depends on the distance scale considered for the surrounding galaxies. Section 6 will lay out the dependence of alignment on other properties such as the number of surrounding galaxies, and magnitude and direction of the mean position offset of the surrounding galaxies. Lastly, Section 7 will summarize the main results and discuss the implications and some future work.

[5]Joachimi et al. 2015; Peebles 1969; Hoyle 1951.

[6]Gunn 1967; Okumura and Jing 2009.

2 Data Source & Color-Magnitude Divider

Using CasJobs [7], I downloaded the data for all galaxies from Data Release (DR) 15 of the Sloan Digital Sky Survey (SDSS)[8,9]. The SDSS imaging survey covered $14,555$ deg^2, roughly one-third of the full sky, recording imaging data for 50 million galaxies and spectroscopic data for 1.5 million of those galaxies[10]. Target galaxies in my study are from the spectroscopic portion of the survey and have precise spectroscopic redshifts.

The redshift range for the galaxies in the SDSS is large, but for the purposes of this study, I limited that range to $0.02 < z < 0.25$. The upper limit at $z = 0.25$ is sufficiently low so that the weak lensing effects are small. The lower limit at $z = 0.02$ is sufficiently large so that the primary source of redshift is the cosmological redshift and not the peculiar motion of the galaxy.

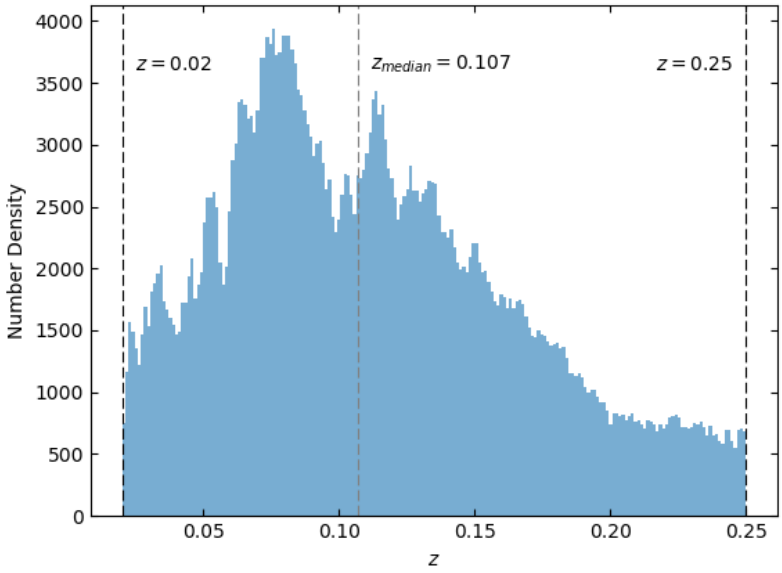

Figure 2.1: Target galaxies redshifts. This figure shows the redshift distribution of the target galaxies. The lower bound, the upper bound, and the median value are marked on the histogram.

The SDSS camera imaged the galaxies in five broadband filters (*ugriz*). This gives the apparent magnitude of an object in each of the five bands. I used photometry in the r and

[7] https://skyserver.sdss.org/casjobs/
[8] Aguado et al. 2019.
[9] https://www.sdss.org/dr15/
[10] Eisenstein et al. 2011.

the u bands with effective wavelengths of $\lambda_r = 6222\mathring{A}$ and $\lambda_u = 3540\mathring{A}$ to get the color and the absolute magnitude[11]. At the (low) redshifts of my sample, the K-correction for magnitudes is small enough to be neglected, especially for r-band. The limiting apparent r-band magnitude for the SDSS spectroscopic survey is $r = 17.7$[12]. There exist galaxies in the spectroscopic survey with $r > 17.7$ (see left-hand panel of Figure 2.2) but the spectroscopic data are not complete at these fainter magnitudes. The SDSS pipeline assigns the value of $r = 24.80$ and $u = 24.63$ to the objects with near-zero flux in the respective bands. This can be seen in the histograms in Figure 2.2. To avoid these zero-flux galaxies, I further limited my sample to only galaxies with $r < 24.4$ and $u < 24.25$ which removed the survey artifacts. Calculating the magnitude difference between two filters gives the color of the object. In

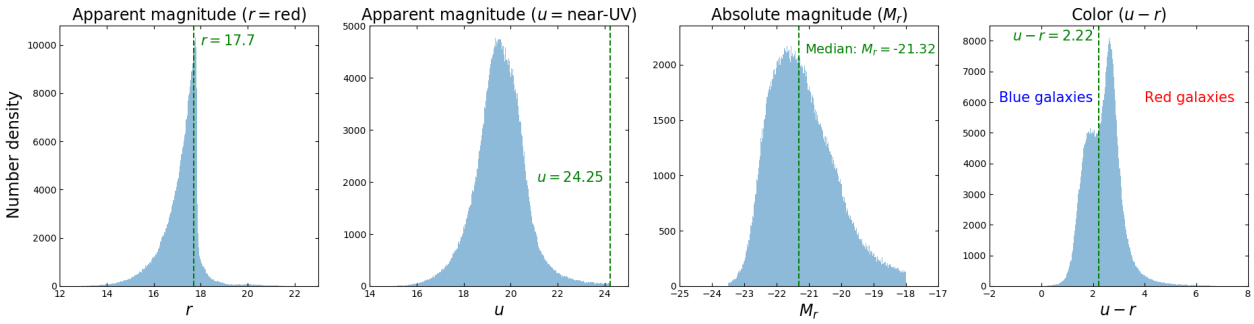

Figure 2.2: Photometric data for the target galaxies. The leftmost panel shows the distribution of r-band magnitudes, where the $r = 17.7$ cutoff for the complete spectroscopic survey is clearly notable. The second panel shows the distribution of the u-band magnitudes. The third panel shows the distribution of the absolute r-band magnitudes with the median value. The rightmost panel shows the distribution of the $u - r$ color index. $u - r = 2.22$ divides the two distinct peaks.

this study, I defined the "color" of a galaxy by the $u - r$ color index. This is particularly convenient because the u-band is sensitive to the presence of hot stars which have strong UV emission. The $u - r$ color index is a good diagnostic of the presence of recent star formation. Using this color index, I can separate the early-type and the late-type galaxies. For a more robust separation, I need the absolute magnitudes of the target galaxies. At low redshift, the relation between distance modulus $r - M_r$ and redshift z is given by[13]

$$r - M_r \approx 43.23 - 5\log_{10}\left(\frac{H_0}{68\ \mathrm{km\,s^{-1}\,Mpc^{-1}}}\right) + 5\log_{10} z + 1.086\,(1 - q_0)\,z, \qquad (2.1)$$

[11]Smith et al. 2002; Fukugita et al. 1996.
[12]Strauss et al. 2002.
[13]Ryden 2017.

where r is the apparent r-band magnitude and M_r is the absolute magnitude, H_0 is the Hubble constant for which I will use $H_0 = 70\ \mathrm{km\,s^{-1}\,Mpc^{-1}}$, and q_0 is the deceleration parameter for which I use the accepted value from the Benchmark Model[14], $q_0 \approx -0.53$. Using these values, equation (2.1) reduces to

$$M_r = r - 43.23 - 5\log_{10} z - 1.662z, \tag{2.2}$$

where z is the spectroscopic redshift of the target galaxy from the SDSS database. The absolute magnitudes computed from equation (2.2) are an indication to how luminous a galaxy is, and I will use M_r as a proxy for a galaxy's luminosity. For concreteness, and to avoid non-galaxy objects, I restricted the absolute magnitudes of target galaxies to $-23.5 \leq M_r \leq -18$. After making all these cuts on several parameters, my final sample contained 385,245 target galaxies.

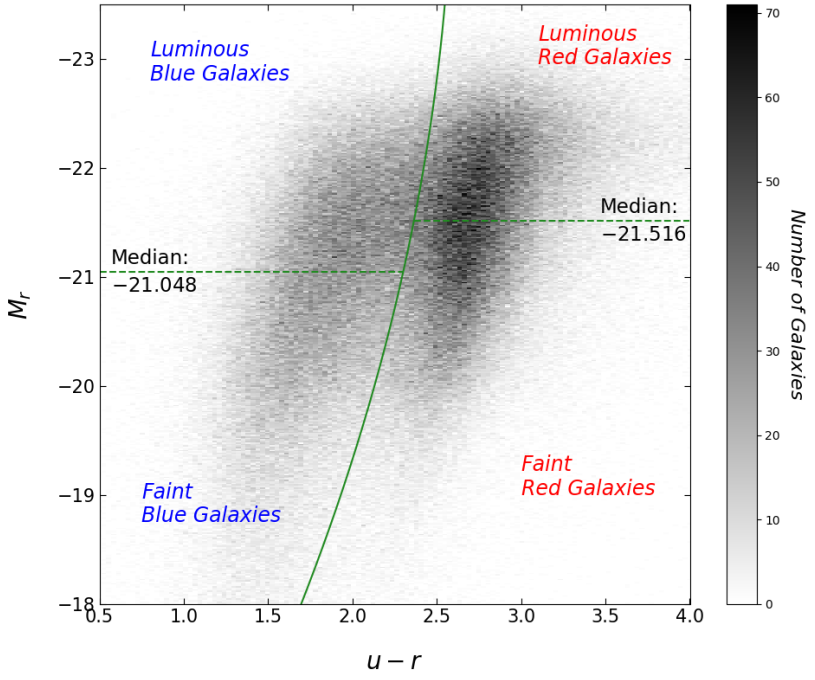

Figure 2.3: Color-magnitude plot and subsamples. The target galaxies are plotted on a $u-r$ color-magnitude plot and divided into red and blue using a magnitude dependent color divider[15]. The red and blue samples are further divided into luminous and faint subsamples using their respective medians.

I further split the final sample using the color divider specified as follows[16]

$$u - r = -0.0178M_r^2 - 0.146M_r + 2.294. \tag{2.3}$$

[14]Ryden 2017.
[16]James and Ryden 2017.

This luminosity-dependent color divider separates blue and red galaxies better than dividing at a constant color index. This division allows me to investigate the dependence of alignments on target galaxy properties such as color and luminosity. The target galaxies that I use in this study are shown as points on the color-magnitude plot in Figure 2.3 along with equation (2.3) to divide blue and red galaxies. Finally, I divided the blue and red galaxies into luminous and faint at their respective medians. Thus, the four sub-samples consist target galaxies of the following properties: Luminous Red (LR), Faint Red (FR), Luminous Blue (LB), and Faint Blue (FB). LR sample and FR sample each have 109,097 target galaxies; LB sample and FB sample each have 83,525 target galaxies.

Position angles (PA) are a convention of defining angles and orientations on the sky where φ increases from North towards East in the sky. PA defined in the SDSS database have a range $-87^\circ \lesssim \varphi \lesssim 246^\circ$. In the database, an image of a galaxy is approximated as an ellipse and since an angular range of 180° is sufficient to describe all possible orientations of an ellipse, I converted all the PA to be within the range $0^\circ < \varphi < 180^\circ$.

The SDSS database also provides the axis ratio for the image of a galaxy. This axis ratio, $0 \leq q \leq 1$, is the measure of how elongated a galaxy is. The more circular a galaxy, the closer q is to 1 and circular shapes don't have well-defined orientations. So, the position angles for galaxies with $q \approx 1$ are not well-defined. On the other extreme, $q \approx 0$ means that the shape of the object is essentially a straight line and is most likely a diffraction spike from a bright star misidentified as a galaxy. In order to eliminate such artifacts, I removed objects with $q < 0.1$ from my data. The distribution of the remaining q for each of the four subsamples is shown in Figure 2.4. It shows that both red and blue luminous samples have the peak q closer to 1 indicating that they are likely 3D ellipsoids with three different axis lengths viewed from different angles. The faint samples have a more uniform distribution indicating their higher abundance of disk-like or flat shapes.

Each target galaxy has its associated "surrounding galaxies." These are galaxies within a projected distance of 30 Mpc of the target galaxy. Projected distance r_p is defined by the equation

$$r_p = 1.25 \text{ Mpc} \left(\frac{z}{0.1}\right) \left(\frac{\theta}{1 \text{ arcmin}}\right), \tag{2.4}$$

where z is the redshift of the target galaxy, and θ is the angular separation in arcsec on the sky. Substituting $r_p = 30$ Mpc in equation (2.4) and solving for the angle θ that corresponds to 30 Mpc at the target galaxy's redshift z, we get

$$\theta = \left(\frac{0.1}{z}\right) \left(\frac{30 \text{ Mpc}}{1.25 \text{ Mpc}}\right) \text{arcmin} = 24 \text{ arcmin} \left(\frac{0.1}{z}\right). \tag{2.5}$$

I carefully selected my target galaxies from the survey regions of the SDSS such that each

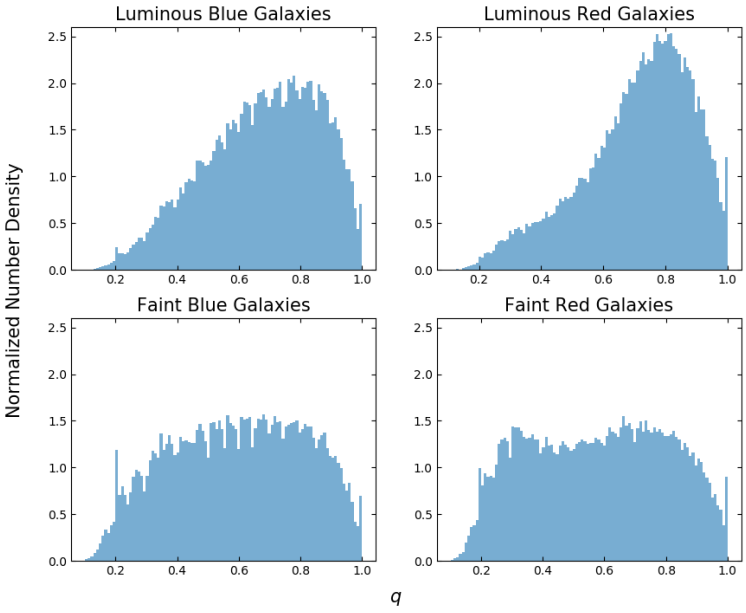

Figure 2.4: Target galaxies axis ratios. The distribution of axis ratio q is shown for the four subsamples of target galaxies. Both luminous subsamples show larger number of target galaxies with q close to 1. The faint subsamples show a more uniform distribution.

target galaxy would have a sufficiently surveyed region to include at least 30 Mpc around the target galaxy. To avoid the boundary of the survey region, I limited the right ascension (RA) and declination (DEC) ranges of my sample of target galaxies to an area within the main region of the survey with a buffer of $\sim 5^\circ$ at the boundaries. This resulted in a sample of galaxies all being located in the same patch of the sky. However, there is no loss of generality here due to the cosmological principle. At the median redshift of the target galaxies, $z \sim 0.1$, an angle $\theta = 1^\circ$ corresponds to a projected distance $r_p \sim 75$ Mpc; thus, the patch of sky I am using ($120^\circ \times 45^\circ$) corresponds to a region 9000 Mpc $\times$ 3375 Mpc, large enough that the cosmological principle applies. We can expect the same properties and behavior at such large scales in any other patch of the sky.

Since the surrounding galaxies are taken from the imaging survey with no spectra, their photometric redshifts z_{surr} are not as accurate as spectroscopic redshifts of the target galaxies. For the surrounding galaxies to be within 30 Mpc of a target galaxy, they need to have redshifts similar to the target galaxy. Keeping in mind the large errors on z_{surr}, I picked surrounding galaxies such that $|z - z_{surr}| < 0.08$, which uses a bound of twice the standard deivation in z_{surr} given z.

3 Defining the Alignment Angle

Alignment studies are done in many ways, with many different definitions of the alignment angle[17], which makes it important to precisely define what I mean by the alignment angle. Prior to that, I need to define and quantify all other relevant properties of a target galaxy and its surrounding galaxies. Suppose that a target galaxy is at right ascension α_t and declination δ_t. It is surrounded by a population of N galaxies that I have designated as "surrounding galaxies," after doing cuts on location and redshift. The i^{th} surrounding galaxy has right ascension α_i and declination δ_i. Since the surrounding galaxies are in small patches of the sky around each target galaxy, I can safely use equation (2.5) and the "flat celestial sphere" approximation, and adopt a Cartesian coordinate system whose origin is at $(\alpha_t,\ \delta_t)$. The x-axis lies in the North-South direction, and the value of x increases going northward; this matches the convention that DEC increases going northward. The y-axis lies in the East-West direction, and the value of y increases going eastward; this matches the convention that RA increases going eastward. The position of each surrounding galaxy, in angular units, is given by $x_i = \delta_i - \delta_t$ and $y_i = (\alpha_i - \alpha_t)\cos\left(\frac{\delta_i+\delta_t}{2}\right)$. Some basic properties of a collection of points on a Cartesian plane are the first and the second moments. Weighing each galaxy equally, the mean offset (first moment) of the surrounding galaxies from the target galaxy in angular units is given by:

$$\mu_x = \frac{1}{N}\sum_{i=1}^{N} x_i \tag{3.1}$$

$$\mu_y = \frac{1}{N}\sum_{i=1}^{N} y_i \tag{3.2}$$

The mean offsets in equations (3.1) and (3.2) only depend on the position of the surrounding galaxies; they do not depend on any other properties of the surrounding galaxies such as the mass or the luminosity.

The mean square offsets (second moments) relative to the center of the distribution of surrounding galaxies are given by:

$$\mu_{xx} = \frac{1}{N}\sum_{i=1}^{N} (x_i - \mu_x)^2 \tag{3.3}$$

$$\mu_{yy} = \frac{1}{N}\sum_{i=1}^{N} (y_i - \mu_y)^2 \tag{3.4}$$

$$\mu_{xy} = \frac{1}{N}\sum_{i=1}^{N} (x_i - \mu_x)\,(y_i - \mu_y). \tag{3.5}$$

[17] Joachimi et al. 2015.

In equations (3.3), (3.4), and (3.5), if $\mu_{xy} = 0$, then the distribution of surrounding galaxies can be approximated as an ellipse whose long axis is along the x-axis (if $\mu_{xx} > \mu_{yy}$) or along the y-axis (if $\mu_{yy} > \mu_{xx}$). If $\mu_{xy} \neq 0$, the distribution of galaxies can be approximated as a tilted ellipse.

The position angle φ_{surr} of this tilted ellipse is given by the relation

$$\tan\left(2\varphi_{surr}\right) = \frac{2\mu_{xy}}{\mu_{xx} - \mu_{yy}} \equiv \beta. \tag{3.6}$$

However, in computing the position angle φ_{surr}, it is important to chose the correct branch of the tangent function. Using the usual convention (North through East) and equation (3.6), the position angle of the ellipse describing the surrounding galaxies is

$$\varphi_{surr} = \frac{1}{2}\tan^{-1}\beta, \qquad [\mu_{xx} > \mu_{yy},\ \mu_{xy} > 0] \tag{3.7}$$

$$\varphi_{surr} = \frac{1}{2}\left(180^\circ + \tan^{-1}\beta\right), \qquad [\mu_{xx} < \mu_{yy}] \tag{3.8}$$

$$\varphi_{surr} = \frac{1}{2}\left(360^\circ + \tan^{-1}\beta\right), \qquad [\mu_{xx} > \mu_{yy},\ \mu_{xy} < 0] \tag{3.9}$$

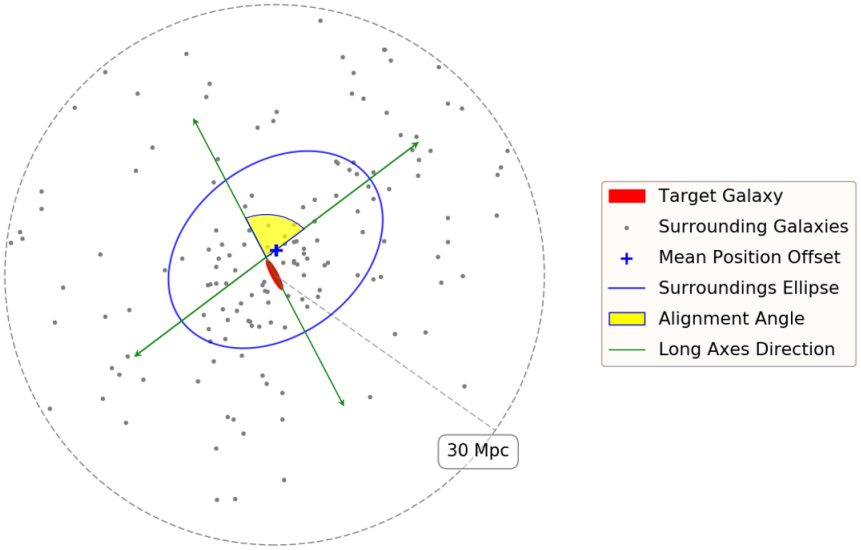

Figure 3.1: Definition of the alignment angle. This illustration shows an example target galaxy in red and its surrounding galaxies as gray dots. The blue ellipse best describes the distribution of the surrounding galaxies. The angular difference between the major axis of that ellipse and the major axis of the target galaxy is defined as the alignment angle, shaded in yellow. The blue cross is the mean position offset of the distribution of surrounding galaxies from the target galaxy.

This position angle φ_{surr} is such that $0° < \varphi_{surr} < 180°$ and indicates the direction of a filament of the large-scale structure if the target galaxy happens to be in one. The mean square moment along the long axis of the ellipse is

$$\mu_{aa} = \frac{1}{2}\left(\mu_{xx} + \mu_{yy} + \sqrt{4\mu_{xy}^2 + (\mu_{xx} - \mu_{yy})^2}\right) \tag{3.10}$$

and the mean square moment along the short axis is

$$\mu_{bb} = \frac{1}{2}\left(\mu_{xx} + \mu_{yy} - \sqrt{4\mu_{xy}^2 + (\mu_{xx} - \mu_{yy})^2}\right). \tag{3.11}$$

Using equations (3.10) and (3.11), the axis ratio q_{surr} of the ellipse describing the surrounding galaxies is then

$$q_{surr} = \sqrt{\frac{\mu_{bb}}{\mu_{aa}}}. \tag{3.12}$$

Now equipped with the necessary geometric tools, I define the alignment angle ϕ as the angular difference between the position angle of the target galaxy φ and the position angle of the ellipse describing the surrounding galaxies φ_{surr} such that $0° \leq \phi \leq 90°$. An illustration of this alignment angle can be seen as the yellow angle between the two green lines in Figure 3.1. This definition of the alignment angle ϕ is used throughout this study.

4 Primary Alignment Analysis

After dividing the main sample into four subsamples based on color and luminosity of the target galaxies, and precisely defining the alignment angle, I can begin to analyze the data. Before doing anything more complex, the simplest analysis is to get the statistics of the datasets. If the sample is randomly distributed, meaning there is no preferred alignment, then the average angle alignment will be 45°. Looking at the results in Table 4, clearly the LR galaxies subsample have the lowest mean with the highest significance, showing a trend toward parallel alignment on average. The FR galaxies subsample's mean is also less than 45°, but with a lower significance. The LB and FB galaxies subsamples have a mean consistent with 45°, showing no preferred alignment. These results already show that red target galaxies, especially the LR galaxies, have a slight preference toward parallel alignment, whereas the blue target galaxies align randomly with their respective surrounding distribution of galaxies. The number of red galaxies is greater than the number of blue galaxies, which results in slightly better error of the mean for the red galaxies.

To further quantify the results and see the trends visually, I plotted a binned histogram for each subsample with 0.5° bins and normalized the x-axis by dividing the alignment

Table 4.1. Simple Alignment Statistics

Galaxy Sample	Mean Alignment Angle	Est. error of mean	No. of target galaxies
Luminous Blue	45.044°	0.090°	83525
Faint Blue	44.992°	0.090°	83525
Luminous Red	44.271°	0.079°	109097
Faint Red	44.684°	0.079°	109097

angles by 90° in order to make it range from dimensionless 0 to 1. In Figure 4.1, 0 on the x-axis shows perfectly parallel alignment and 1 shows perfectly perpendicular alignment of the target galaxy with its surrounding distribution of galaxies. To model the trend in the histogram, a linear fit was the best choice since the spread in the data is large and fitting with a polynomial of any higher order would just be absurd. The frequency of occurrence is normalized to $y = 1$ at $x = 0.5$ (i.e. 45°); this eliminates the 'intercept' parameter in a linear fit, making the slope the only relevant fit parameter.

I get the best fitting slopes for all four subsamples by doing a simple linear least-squares fit using Python. The corresponding results for each subsample are shown in Figure 4.1. After fitting the data, I vary the slope and perform the Kolmogorov-Smirnov (K-S) test on the results to find the 90% two-sided confidence level in the slope. The K-S test compares two cumulative distribution functions (CDF) by quantifying the largest distance between the CDF of a data sample and some reference CDF. If the two distributions are identical, they follow the null hypothesis and the largest distance is zero. The K-S test also provides a p-value which I used to signify the 90% two-sided confidence level in the best-fit slopes. For my analysis, I compare my data with a random distribution to see how much the distribution of alignment angles deviates from random distribution. Here again, the LR galaxies subsample has the most negative slope with the highest significance, indicating the overabundance of galaxies with a parallel alignment with their surroundings. Slopes of both the blue subsamples are consistent with being zero with at least 90% confidence, confirming the random distribution of alignment angles. The FR galaxies subsample also has a slightly negative slope which is still significant at the 90% confidence level.

For a more detailed understanding of dependence of alignment on luminosity, instead of dividing up the target galaxies into four subsamples based on their color and luminosity, I plotted the average alignment angle for the red and blue samples as a function of 1% lumi-

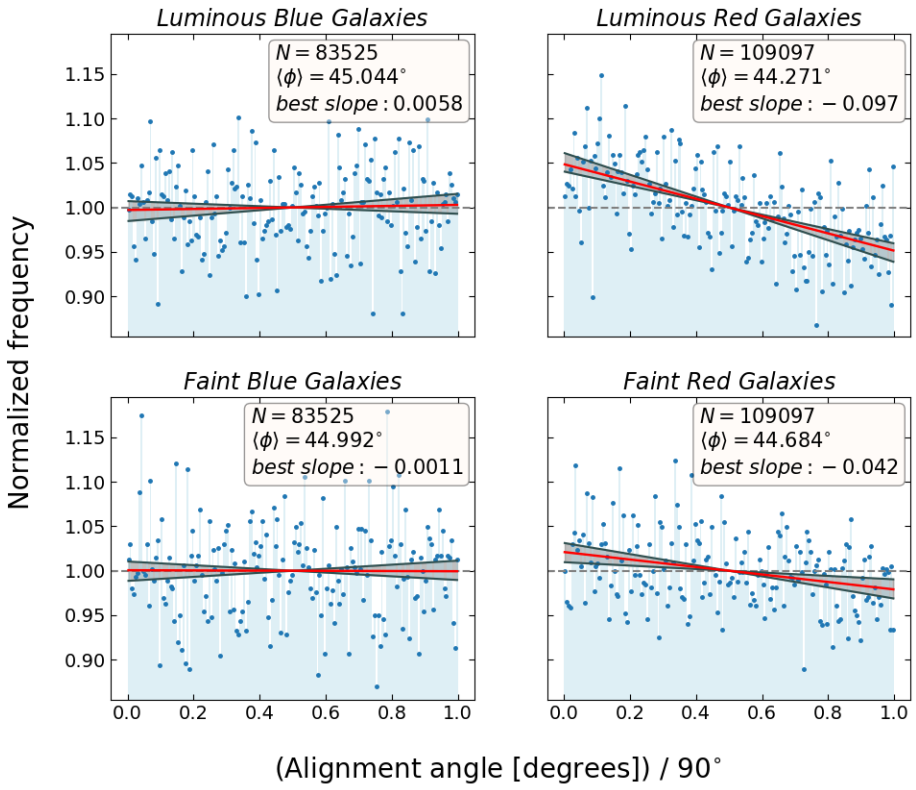

Figure 4.1: Alignment angle distribution. This plot shows the normalized histograms of the alignment angle for all four subsamples. The left two panels display the random distribution of alignment angle for the blue galaxies. The top-right panel is the most significant (9σ) result and it shows that the luminous red galaxies have an average parallel alignment with their surroundings. The bottom-right panel shows parallel alignment also for the faint red galaxies, but the significance is lower (4σ).

nosity bins in Figure 4.2. The blue sample showed an average alignment of 45° throughout the luminosity bins except for the most luminous 3-4%. In the red sample, there was a clear trend going from the most luminous to the least luminous galaxies. More luminous galaxies showed a stronger parallel alignment.

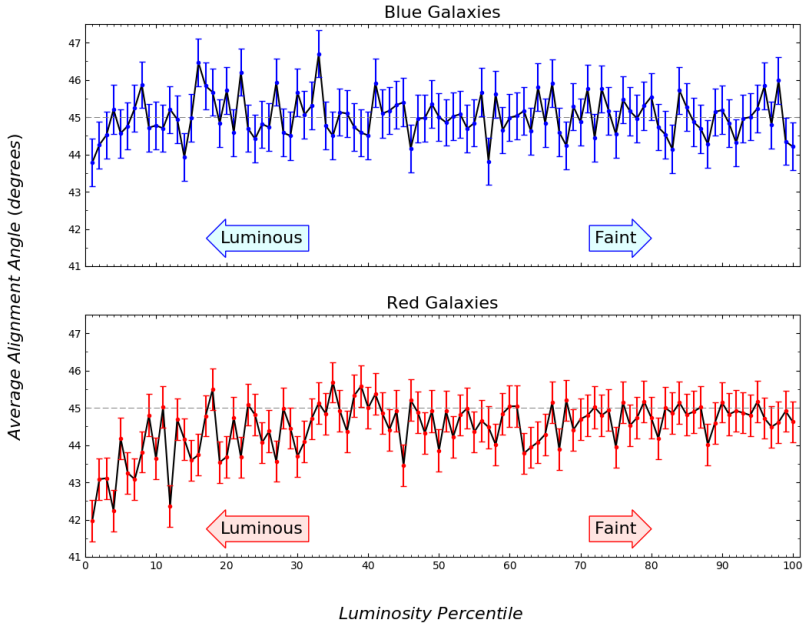

Figure 4.2: Average alignment as a function of luminosity. In effect, the x-axis is the luminosity of the target galaxy and the y-axis is the average alignment angle in the respective luminosity bin. There is no significant trend for the blue target galaxies in the top panel, but the red galaxies in the bottom panel show a clear trend of alignment being significantly parallel at high luminosities.

5 Varying the Surrounding Radius

The results in the previous section show alignment of the target galaxy with the distribution of their surrounding galaxies within 30 Mpc of the target galaxy. Now instead of considering surrounding galaxies within only 30 Mpc, I vary the surrounding radius r_p from 5 to 30 Mpc. This allows to investigate any trend in the alignment angle as a function of the surrounding radius, the distance scale being considered. The lower limit of 5 Mpc is a reasonable one because for $r_p \geq 5$ Mpc, the number of surrounding galaxies within that radius is at least 3 and the ellipse describing the distribution of surrounding galaxies can be

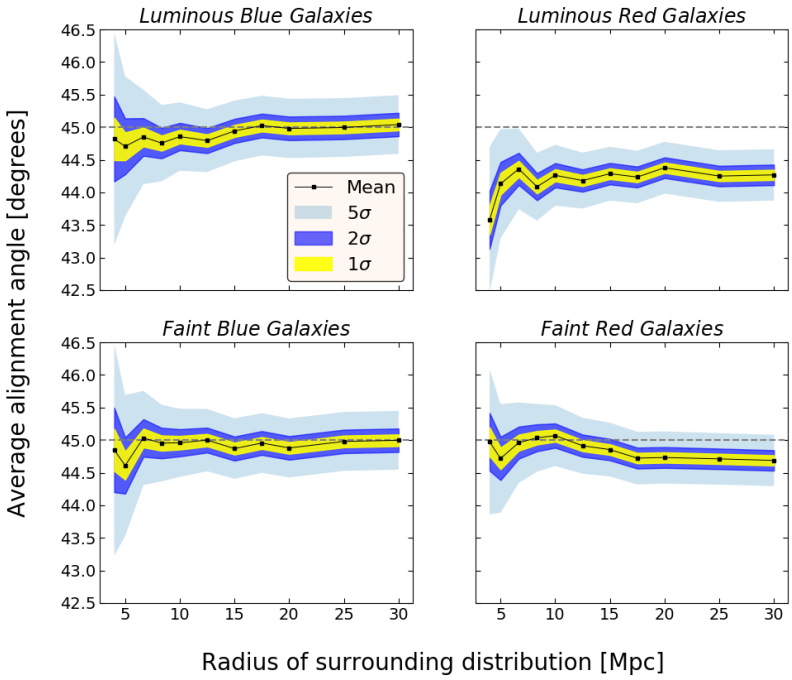

Figure 5.1: Alignment vs. surrounding radius. This plot shows the average alignment angle as a function of surrounding radius (5 Mpc $\leq r_p \leq$ 30 Mpc) for all four subsamples. The left two panels display the average alignment consistent with 45° for the blue galaxies at any r_p. The top-right panel shows that the luminous red galaxies have an average alignment of $\langle\phi\rangle \approx 44.3°$ throughout the range of r_p. The bottom-right panel for the faint red galaxies shows that the average alignment angle is consistent with 45° for $r_p \lesssim 18$ Mpc and it is parallel for $r_p \gtrsim 18$ Mpc.

well-defined. In Figure 5.1, I plot the average alignment angle for surrounding radii between 5 and 30 Mpc. The error on each point is from standard error of the mean (σ) of each bin and I have shown errors up to 5σ. Again, both the blue subsamples are consistent with 45° average alignment angle regardless of the surrounding radius, conforming with random distribution. Average alignment angle for the LR galaxies consistently lies below 45°, roughly constant at $\langle\phi\rangle \sim 44.3°$, showing a parallel alignment at any value of the surrounding radius. The significance of this result, how far the mean is from the 45° mark, is 9σ for the largest surrounding radius. Average alignment angle for the FR galaxies is consistent with 45° up to $\sim$ 18 Mpc, and for surrounding radii larger than that, there is a parallel alignment at 4σ significance. 18 Mpc is close to the mean distance between moderately large galaxy clusters, meaning the result for the faint red galaxies could be related to that, but more data are needed to confirm this.

6 Dependence of Alignment on Other Properties

Following the main analyses of this study, I also performed some secondary analyses on alignments to further investigate the dependence of alignment on other properties. Firstly, I investigated how the alignment depends on the number of surrounding galaxies. I normalized the number of surrounding galaxies by the mean number of surrounding galaxies in the target galaxy's redshift bin. This average number of surrounding galaxies is shown as a function of redshift in Figure 6.1. As shown in Figure 6.2, I binned and plotted the alignment angle

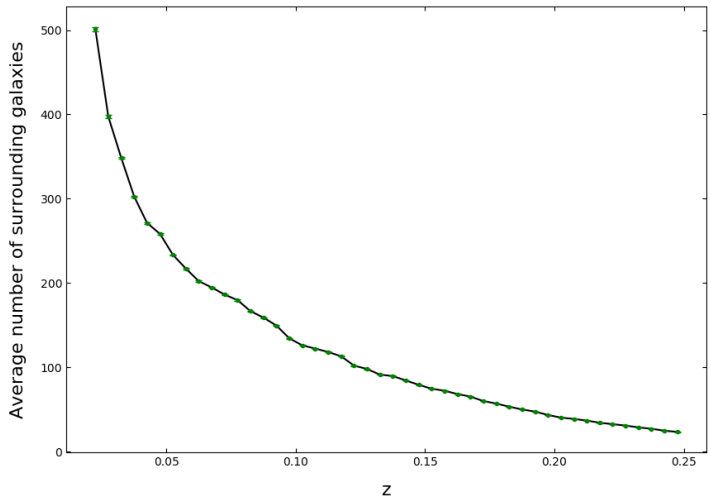

Figure 6.1: Average number of surrounding galaxies vs. redshift. The binned data for the average number of surrounding galaxies for a given redshift bin are shown in this plot.

as a function of the normalized number of surrounding galaxies. For the most under-dense bin in the luminous blue subsample, there are only two target galaxies and both happen to have very similar alignment angles making the error on that bin small. So, this bin cannot be regarded as a significant result. Considering this, all four subsamples have no significant alignment trends as a function of the number of surrounding galaxies.

Next, I considered the alignment as a function of mean offset of the surrounding galaxy distribution. The mean offset of a sample of surrounding galaxies is the mean of their positions in a Cartesian coordinate system as defined in equations (3.1) and (3.2). Dividing the mean offset by the surrounding radius (30 Mpc), I made it a fractional offset. I sorted, binned, and plotted the alignment angle as a function of the fractional offset in Figure 6.3 and again saw that there were no significant trends.

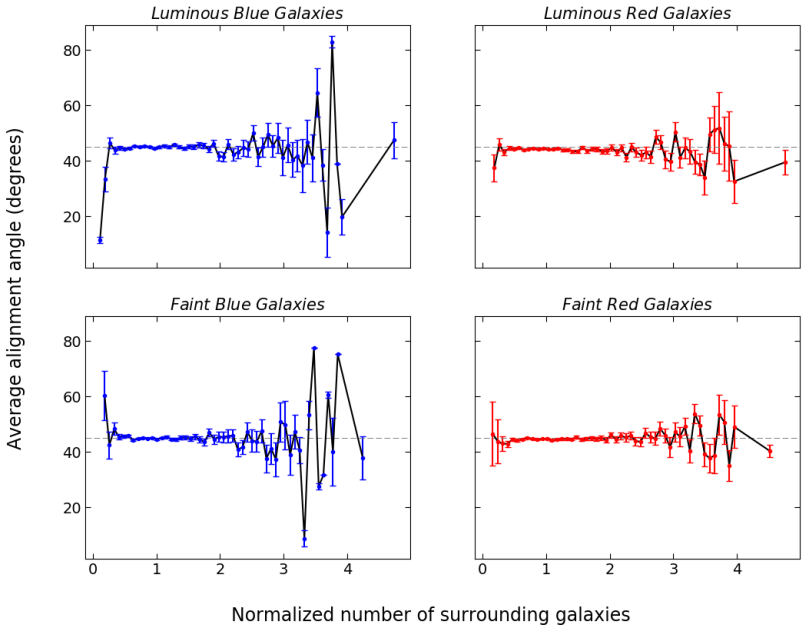

Figure 6.2: Average alignment vs. number of surrounding galaxies. This plot illustrates that for all four subsamples, there are no significant trends in alignment as a function of the number of surrounding galaxies.

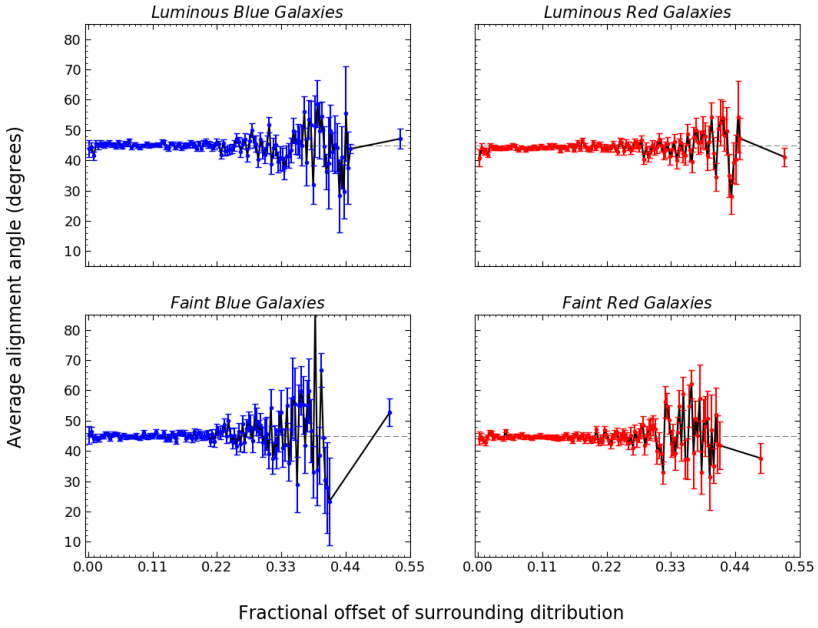

Figure 6.3: Average alignment vs. fractional offset. This plot illustrates that for all four subsamples, there are no significant trends in alignment as a function of the fractional mean offset of the surrounding galaxies from the target galaxy.

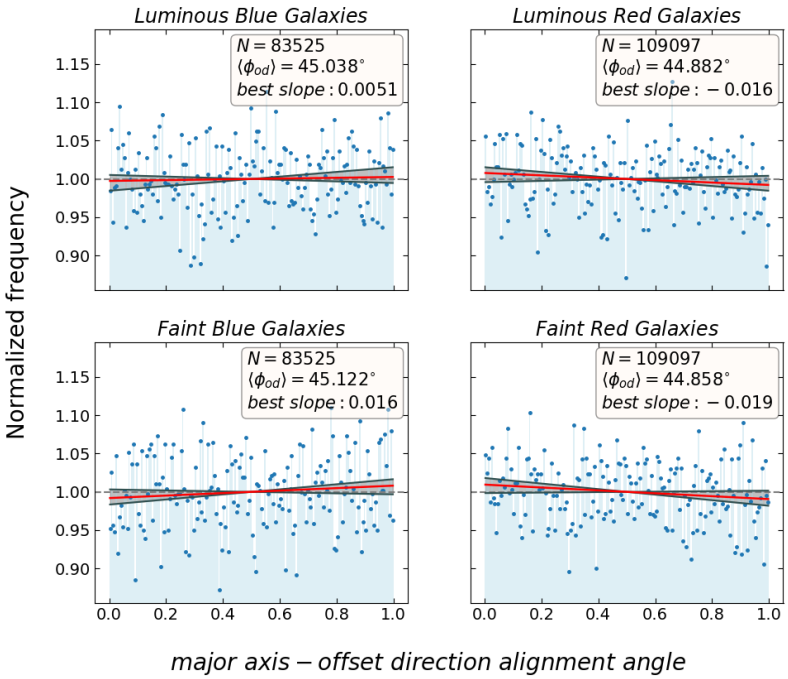

Figure 6.4: Alignment with the direction of offset. This plot shows the normalized histograms of the alignment with the offset direction for all four subsamples. All four subsamples display the random distribution of alignment angle, showing that there is no preferred alignment of the major axis of a galaxy with the direction of offset from its surrounding galaxies.

From Figure 6.3, it is clear that the alignment doesn't depend on the magnitude of the mean offset. To determine the dependence of alignment on the direction of the mean offset, I define an alignment angle ϕ_{od} different from the one previously defined and create a plot similar to Figure 4.1 and perform the same statistical analyses on the subsamples. This new alignment angle is the one between the major axis of the target galaxy and the direction of the previously defined mean offset from the target galaxy. It shows how well the target galaxy aligns with the direction of the mean offset, the clumping of the surrounding galaxies. It answers the question: if the target galaxy is offset from a cluster of dimmer galaxies, does it tend to "point" to the nearby cluster? In Figure 6.4, all four subsamples show a best-fit slope consistent with zero at a 90% confidence level specified by the K-S test. This new alignment angle is thus randomly distributed across all galaxies, with no preference towards parallel or perpendicular alignment. So, the answer to the proposed question is: no, the target galaxy does not tend to "point" to the nearby cluster; on average, these alignments are random.

7 Discussion & Conclusion

In this thesis research, I studied the alignment of galaxies with their surrounding distribution of galaxies and its dependence on several properties. For this, I used spectroscopic galaxies as my target galaxies and photometric galaxies as my surrounding galaxies from the SDSS DR15[18,19]. The primary analysis of the alignment angle on the four color-luminosity subsamples showed that the luminous red galaxies have a preferred parallel alignment with their surrounding distribution with $\langle\phi\rangle = 44.27^\circ \pm 0.08^\circ$. This result is significant at a 9σ level. Faint red galaxies also showed preferred parallel alignment, but at a lower significance (4σ) with $\langle\phi\rangle = 44.68^\circ \pm 0.08^\circ$. This conforms with the overview by Joachimi et al showing that the red galaxies tend to align their major axes with the filament direction[20]. Both the blue subsamples in my study have alignments consistent with 45° meaning that there is no preferred direction of alignment. Blue galaxies tend to be disk-shaped, late-type galaxies which are angular momentum supported. Some studies have shown that their angular momentum vector (or spin vector) tends to lie perpendicular to the filament direction[21]. However, my analysis does not show any significant alignments for blue galaxies; the angular momentum vector does not seem to be aligned with the large-scale structure.

The result that the blue galaxies show no average alignment is important for weak-lensing surveys. To catch the weak signal from the weak-lensing events, the galaxies in the field must be shown to have little-to-no intrinsic alignment. So, blue target galaxies can be used for weak-lensing surveys. Of course, there are issues with throwing away all the red galaxies, which make up more than half of the total galaxies. Possibly incorporating the alignments seen for the red galaxies into the weak-lensing equations might provide a better solution. The alignment of the red, especially luminous galaxies can be useful in studying the formation and evolution of the large-scale structure. As a next step, similar statistical alignment analyses can be done on galaxies using simulations along with observations. This gives the freedom of choosing different viewing angles, drawing a more complete 3D picture, and changing several parameters to see their effects on alignments. Although having several issues such as the observational limits and galaxy population biases at higher redshifts, investigating alignment as a function of redshift for different types of galaxies is another interesting study that can be done.

[18] Aguado et al. 2019.
[19] https://www.sdss.org/dr15/
[20] Joachimi et al. 2015.
[21] Ibid.

References

Aguado, D. S. et al. (Feb. 2019). "The Fifteenth Data Release of the Sloan Digital Sky Surveys: First Release of MaNGA-derived Quantities, Data Visualization Tools, and Stellar Library". In: *Astrophysical Journal, Supplement* 240.2, 23, p. 23. DOI: 10.3847/1538-4365/aaf651. arXiv: 1812.02759 [astro-ph.IM].

Brown, F. G. (Apr. 1939). "The distribution of the position-angles of the extra-galactic nebulæ in Horologium". In: *Monthly Notices of the Royal Astronomical Society* 99, p. 534. DOI: 10.1093/mnras/99.6.534.

— (Jan. 1964). "Classified forms and position angles of 4891 galaxies in a continuous field of 3071 square degrees centred in the Constellation Pisces". In: *Monthly Notices of the Royal Astronomical Society* 127, p. 517. DOI: 10.1093/mnras/127.6.517.

Chen, Yen-Chi et al. (Feb. 2019). "Detecting galaxy–filament alignments in the Sloan Digital Sky Survey III". In: *Monthly Notices of the Royal Astronomical Society* 485.2, pp. 2492–2504. ISSN: 0035-8711. DOI: 10.1093/mnras/stz539. eprint: https://academic.oup.com/mnras/article-pdf/485/2/2492/28030693/stz539.pdf. URL: https://doi.org/10.1093/mnras/stz539.

Eisenstein, Daniel J. et al. (Sept. 2011). "SDSS-III: Massive Spectroscopic Surveys of the Distant Universe, the Milky Way, and Extra-Solar Planetary Systems". In: *Astronomical Journal* 142.3, 72, p. 72. DOI: 10.1088/0004-6256/142/3/72. arXiv: 1101.1529 [astro-ph.IM].

Fukugita, M. et al. (Apr. 1996). "The Sloan Digital Sky Survey Photometric System". In: *Astronomical Journal* 111, p. 1748. DOI: 10.1086/117915.

Ganeshaiah Veena, Punyakoti et al. (May 2019). "The Cosmic Ballet II: spin alignment of galaxies and haloes with large-scale filaments in the EAGLE simulation". In: *Monthly Notices of the Royal Astronomical Society* 487.2, pp. 1607–1625. ISSN: 0035-8711. DOI: 10.1093/mnras/stz1343. eprint: https://academic.oup.com/mnras/article-pdf/487/2/1607/32358866/stz1343.pdf. URL: https://doi.org/10.1093/mnras/stz1343.

Gunn, James E. (Dec. 1967). "On the Propagation of Light in Inhomogeneous Cosmologies. I. Mean Effects". In: *Astrophysical Journal* 150, p. 737. DOI: 10.1086/149378.

Hoyle, F. (Jan. 1951). "The Origin of the Rotations of the Galaxies". In: *Problems of Cosmical Aerodynamics*, p. 195.

James, Derrick and Barbara Ryden (2017). "The Green Valley: Separating Galaxy Populations in Color-Magnitude Space".

Joachimi, Benjamin et al. (2015). "Galaxy Alignments: An Overview". In: *Space Science Reviews* 193.1, pp. 1–65. ISSN: 1572-9672. DOI: 10.1007/s11214-015-0177-4. URL: https://doi.org/10.1007/s11214-015-0177-4.

Okumura, Teppei and Y. P. Jing (Mar. 2009). "THE GRAVITATIONAL SHEAR-INTRINSIC ELLIPTICITY CORRELATION FUNCTIONS OF LUMINOUS RED GALAXIES IN OBSERVATION AND IN THE ΛCDM MODEL". In: *The Astrophysical Journal* 694.1, pp. L83–L86. DOI: 10.1088/0004-637x/694/1/l83. URL: https://doi.org/10.1088%2F0004-637x%2F694%2F1%2Fl83.

Peebles, P. J. E. (Feb. 1969). "Origin of the Angular Momentum of Galaxies". In: *Astrophysical Journal* 155, p. 393. DOI: 10.1086/149876.

Reaves, Gibson (Oct. 1958). "The Position Angles of Galaxies in Horologium". In: *Publications of the ASP* 70.416, pp. 461–462. DOI: 10.1086/127270.

Ryden, Barbara (2017). *Introduction to Cosmology*. 2nd. Cambridge University Press.

Smith, J. Allyn et al. (Apr. 2002). "The u'g'r'i'z' Standard-Star System". In: *Astronomical Journal* 123.4, pp. 2121–2144. DOI: 10.1086/339311. arXiv: astro-ph/0201143 [astro-ph].

Strauss, Michael A. et al. (Sept. 2002). "Spectroscopic Target Selection in the Sloan Digital Sky Survey: The Main Galaxy Sample". In: *Astronomical Journal* 124.3, pp. 1810–1824. DOI: 10.1086/342343. arXiv: astro-ph/0206225 [astro-ph].

Wyatt S. P., Jr. and F. G. Brown (Dec. 1955). "Position angles and shapes of galaxies in Cetus". In: *Astronomical Journal* 60, p. 415. DOI: 10.1086/107250.